ESTIMATING MODAL PROPORTIONS OF MAJOR ROCK-FORMING MINERALS IN PIXL TARGETS ON MARS USING SUPERVISED IMAGE CLASSIFICATION. J. Labrie[1], M.E. Schmidt[1], T.V. Kizovski[1], J.D. Hernández-Montenegro[2], A.Y. Li[3], D. Flannery[4], B. Orenstein[4], D.A.K. Pedersen[5], J. Henneke[5], M. Tice[6], J. Hurowitz[7], and A. Allwood[2], [1]Brock U. (St. Catharines, ON L2S 3A1, Canada, jl17dx@brocku.ca), [2]JPL-Caltech (Pasadena, CA 91125), [3]U. of Washington (Seattle, WA 98195), [4]Queensland U. of Technology (Brisbane City QLD 4000, Australia), [5]Technical U. of Denmark (2800 Kongens Lyngby, Denmark), [6]Texas A&M (College Station, TX 77843), [7]SUNY Stony Brook (NY 11794)

Introduction: Reaching Jezero crater, Mars in early 2020 onboard NASA's M2020 Perseverance rover, the Planetary Instrument for X-ray Lithochemistry (PIXL) is an X-ray fluorescence (XRF) spectrometer used to determine the elemental geochemistry of martian surface materials [1]. PIXL helps to fulfill one of the primary objectives of the Mars 2020 mission: to investigate the geological processes that have acted upon Jezero and the Martian surface over the planet's history, a part of the broader search for environments that were once hospitable to life [2]. Combined with context imagery from its multispectral (NIR, G, B, UV) Micro-Context Camera (MCC), which is radiometrically calibrated to absolute radiance values based on pre-flight calibration of the optical system [3,4], PIXL allows for a high-resolution (~125 µm XRF spot size) look at the chemistry and texture of rocks, dust, and regolith across Jezero crater. These data can be viewed and manipulated using PIXLISE [1], a data visualization and analysis software program.

Although Perseverance uses its abrasion and dust removal tools to clear a ~40-50 mm diameter patch of fresh material on target surfaces, PIXL maps generally only represent a relatively small fraction of this area (maps have ranged from 5x5 to 4x12 mm) [1]. While PIXLISE allows researchers to analyze the petrology of PIXL targets in a number of different ways, this analysis is restricted to the small area of PIXL maps, limiting the scale of phase maps and modal analysis.

Here, we develop a methodology for producing phase maps of abrasion patches with freely available machine learning software. Using an image classification algorithm, we produce phase maps for three different PIXL targets, analyze the modal proportions of pyroxene, olivine, and feldspar, and discuss the statistical quality of our output. Our focus here is on igneous lithologies of the Jezero crater floor Séitah (olivine cumulate) and Máaz (Fe-rich basalt) formations [5,6], but analogous techniques may be applied to clastic sedimentary lithologies of the Jezero delta [7].

Methodology: We focus on representative PIXL maps including the relatively coarse-grained Dourbes (M2020 sol 257), Quartier (sol 301), and Montpezat (sol 349) targets, as all three igneous minerals (olivine, pyroxene, feldspar) considered in this study are clearly identified within each PIXL map.

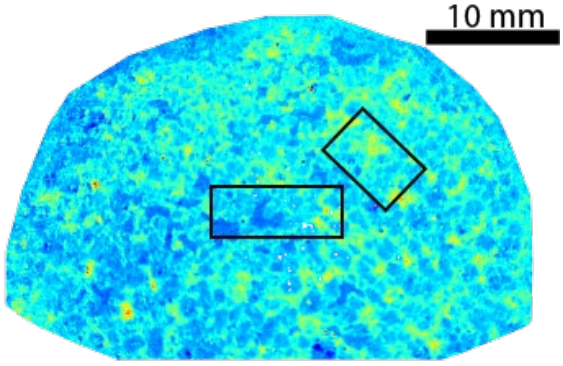

Figure 1: NIR/G spectral ratio MCC image of Dourbes. Image has been cropped from original extent to remove areas of unabraded surface and noise. Black boxes indicate approximate location of PIXL maps.

To determine modal mineralogy, expressions were developed within PIXLISE to identify XRF points representative of chemically ideal mineral endmembers, including pyroxene, olivine, and feldspar. These expressions use molar ratios of various elements to identify specific mineral endmember compositions in PIXL XRF data. For example, the expression for finding pyroxene identifies XRF points where the ratio of (Fe+Mg+Ca) to Si is equal to 1, and the ratio of Si to Al is equal to 3. This technique is complementary to the MIST algorithm [8], and includes XRF points within +/- 10-20% of the stoichiometric ideal for each phase to better account for mixing between XRF spectra.

Once identified, these points were defined as Regions of Interest (ROIs), allowing them to be displayed overtop MCC imagery in PIXLISE. This view was screen-captured and aligned with spectral ratio MCC image stacks (sets of images that show the ratio between different wavelengths; see Figure 1) using Adobe Illustrator. Next, the aligned ROIs and MCC images were imported into XMapTools, a free, MATLAB-based software program used for chemical analysis [9,10]. Within XMapTools, the aligned ROIs were traced and used as training points for a supervised image classification, with MCC ratio images serving as the data set to be analyzed. Using the random forest classification algorithm, the software generated a phase map for each PIXL target, classifying each pixel into one of five phases: (1) pyroxene; (2) olivine; (3) feldspar; (4) other (used for data that cannot be classified as one of the three mineral phases); (5) no data

(used for spots where data is excluded due to overexposure in raw MCC images). Statistical information was also generated to assess the accuracy and robustness of the classification.

Results & Discussion: PIXLISE expressions for recognizing ideal mineral endmembers identified varying numbers of XRF points of each phase in each PIXL map (Table 1). Using these XRF points as training points, the classification algorithm successfully generated a phase map for each PIXL target (Figure 2), allowing for the calculation of modal proportions for each phase (Table 1). The "no data" phase was not included in these calculations.

Table 1: Mineral modal proportions

Target	Mineral Class	% of PMCs in PIXL map *(count)*	Modal % in phase map
Montpezat 2 (2339 XRF points)	***pyroxene***	28.9 *(677)*	75.0
	olivine	1.4 *(33)*	0.9
	feldspar	1.9 *(44)*	1.8
	other	67.8 *(1585)*	22.3
Dourbes (3335 XRF points)	***pyroxene***	16.9 *(563)*	12.7
	olivine	26.2 *(873)*	49.2
	feldspar	1.8 *(61)*	1.1
	other	55.1 *(1838)*	37.0
Quartier 2 (3335 XRF points)	***pyroxene***	32.5 *(1083)*	44.3
	olivine	10.6 *(353)*	21.4
	feldspar	0.2 *(5)*	0.1
	other	56.8 *(1894)*	34.4

Pyroxene and/or olivine were found to be the dominant phases in each of the three maps, with the remainder of the maps mostly comprising other phases, such as Fe-oxide, secondary salts, or other alteration phases. Feldspar had a modal proportion of less than 2% in each phase map. The combined modal proportions of pyroxene, olivine, and feldspar in the phase maps are greater than their initial proportions of XRF points in PIXL maps. The proportion of other phases is less than the initial proportion of XRF points (Table 1). This may suggest that the classification algorithm is able to take training points with ideal phase compositions and use this information to identify members of each phase with "imperfect" compositions (e.g., those that have been weathered or otherwise altered).

Using statistical data generated within XMapTools, the recall (the proportion of correctly predicted samples in a given class) was tabulated for each class in each phase map. This allowed for assessment of the algorithm's ability to confidently identify each phase. Recall for pyroxene, olivine, and other phases was quite high, ranging from 89-100% across all three phase maps. The feldspar class generally had lower recall, ranging from 74-90%. This may indicate a lack of strong feldspar spectral signatures in MCC imagery.

Future work will include additional phases in the overall phase maps, and adjustments to PIXLISE expressions for finer-grained materials. Results will allow for more in-depth, less time-consuming modal analysis of PIXL imaging and scan areas, and quantitative classification of the rocks in Jezero crater.

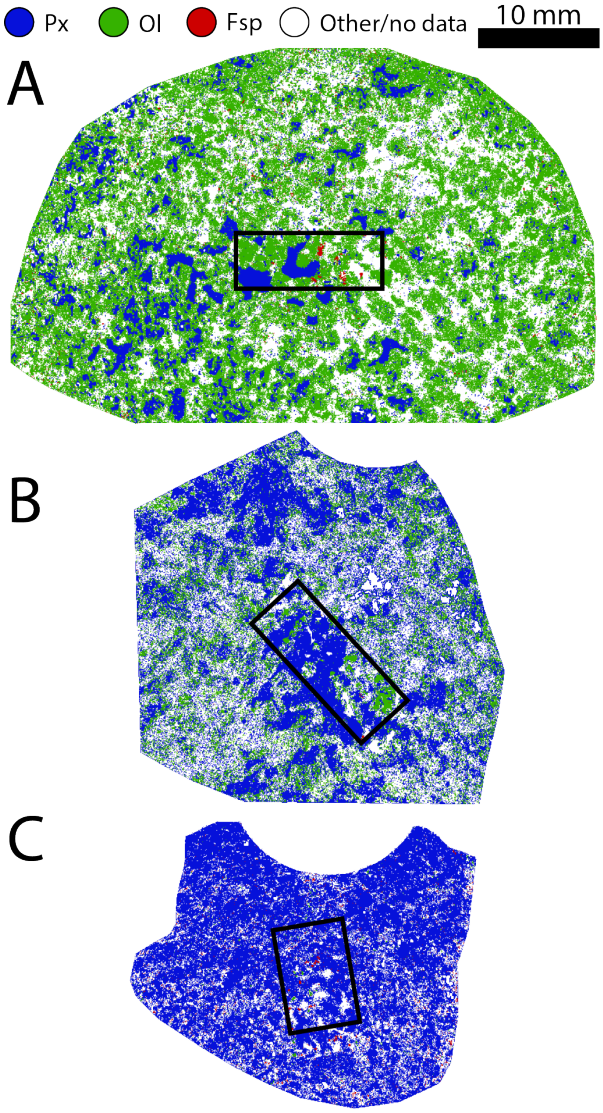

Figure 2: Phase maps for PIXL targets Dourbes (A), Quartier 2 (B), and Montpezat 2 (C). Px = pyroxene, Ol = olivine, Fsp = feldspar. Black boxes indicate approximate location of PIXL map.

References: [1] Allwood, A. C. et al. (2020) *Space Sci. Rev.*, 216(8), 1-132. [2] Boeder, P.A. & Soares, C.E. (2020) *Proceedings SPIE 11489, Systems Contamination: Prediction, Control, and Performance 2020*, 1148903. [3] Pedersen, D.A.K. et al (accepted) *Space Sci. Rev*. [4] Henneke, J. et al. (under review) *Space Sci. Rev.* [5] Farley, K.A. et al. (2022) *Science*, 377. [6] Liu, Y. et al. (2022) *Science*, 377, 1513-1519. [7] Hurowitz, J. et al. (2023) *LPSC LIV* [8] Moreland, E. et al. (2022) *AGU Fall Meeting 2022*, Abstract P55A-06. [9] Lanari, P. et al. (2014) *Computers and Geosciences*, 62, 227-240. [10] Lanari, P. et al. (2019) *Geological Society of London, Special Publications,* 478, 39-63.